RESEARCH ARTICLE

Pattern of Brain Parenchymal Damage Related to Cerebral Small Vessel Disease in Carriers of Rare *NOTCH3* Variants

Zi-Yue Liu, MD, Fei-Fei Zhai, MD, Jing-Yi Liu, MD, Yi-Jun Zhou, MD, Mei-Jun Shu, MD, Xiao-Hong Huang, MD, Fei Han, MD, Ming-Li Li, MD, Li-Xin Zhou, MD, Jun Ni, MD, PhD, Ming Yao, MD, Shu-Yang Zhang, MD, PhD, Li-Ying Cui, MD, PhD, Zheng-Yu Jin, MD, and Yi-Cheng Zhu, MD, PhD

Correspondence
Dr. Zhu
zhuych910@163.com

Neurology® 2023;101:e1979-e1991. doi:10.1212/WNL.0000000000207882

Abstract

Background and Objectives

Previous studies reported that carriers of rare *NOTCH3* variants comprised more than 10% of the general population and are susceptible to a heavy overall burden of cerebral small vessel disease while the injury patterns remain uncovered. This study aimed to investigate the imaging features in relation to rare *NOTCH3* variants and the interaction between cortical atrophy and white matter lesions from a longitudinal view, with respect to spatial and dynamic patterns.

Methods

As part of a community-based cohort, we included participants with complete whole-exome sequencing and brain MRI in the baseline analysis. All participants were invited for a 5-year follow-up MRI, and those who did not complete the follow-up were excluded from the longitudinal analysis. *NOTCH3* variants with minor allele frequency <1% in all 4 public population databases were defined as rare variants. We used general linear models to compare the volume of white matter hyperintensity (WMH) volume and brain parenchymal fraction between rare *NOTCH3* variant carriers and noncarriers. In addition, we compared the WMH probability map and vertex-wise cortex maps at a voxel/vertex-wise level.

Results

A total of 1,054 participants were included in baseline analysis (13.56% carried rare *NOTCH3* variants), among whom 661 had a follow-up brain MRI (13.76% carried rare *NOTCH3* variants). Rare *NOTCH3* variant carriers had a heavier white matter hyperintensity burden (1.65 vs 0.85 mL, $p = 0.025$) and had more extensive WMH distributed in the periventricular areas. We also found that rare *NOTCH3* variant carriers were susceptible to worse cortical atrophy ($\beta = -0.004$, SE = 0.002, $p = 0.057$, adjusted for age and sex). Cortical atrophy of multiple regions in the frontal and parietal lobes was related to white matter hyperintensity progression.

Discussion

Individuals with rare *NOTCH3* variants have a distinct pattern of brain parenchymal damage related to CSVD. Our findings uncover the important genetic predisposition in age-related cerebral small vessel disease in the general population.

From the Department of Neurology (Z.-Y.L., F.-F.Z., M.-J.S., X.-H.H., F.H., L.-X.Z., J.N., M.Y., L.-Y.C., Y.-C.Z.); Department of Radiology (J.-Y.L., Y.-J.Z., M.-L.L., Z.-Y.J.); and Department of Cardiology (S.-Y.Z.), State Key Laboratory of Complex Severe and Rare Diseases, Peking Union Medical College Hospital, Chinese Academy of Medical Sciences and Peking Union Medical College, Beijing, China.

Go to Neurology.org/N for full disclosures. Funding information and disclosures deemed relevant by the authors, if any, are provided at the end of the article.

Glossary

BIANCA = brain intensity abnormality classification algorithm; **BPF** = brain parenchymal fraction; **CADASIL** = cerebral autosomal-dominant arteriopathy with subcortical infarcts and leukoencephalopathy; **CSVD** = cerebral small vessel disease; **EGFr** = epidermal growth factor-like repeats; **GLM** = generalized linear model; **GMF** = gray matter fraction; **IQR** = interquartile range; **MNI** = Montreal Neurologic Institute; **WES** = whole-exome sequencing; **WMF** = white matter fraction; **WMH** = white matter hyperintensity.

Introduction

Cerebral small vessel disease (CSVD) is a common cause of cognitive impairment, gait dysfunction, and stroke, which are affected by various genetic and environmental factors.[1] Accumulating evidence revealed that pathogenic variants known to cause Mendelian forms of CSVD are frequent among the general population, such as the characteristic cysteine-altering variation in the *NOTCH3* gene.[2-4] In addition, our previous study[5] and the study by Schmidt[6] reported the susceptibility to heavy CSVD burden in rare *NOTCH3* variant carriers. As carriers of rare *NOTCH3* variants have been identified in more than 10% of the general population,[5] their patterns of brain parenchymal injury deserve in-depth investigation to uncover the important genetic predisposition in age-related CSVD in the general population.

As proposed in patients with CSVD, white matter hyperintensities (WMHs) in different locations have distinct clinical profiles,[7-9] and WMHs involving pyramidal tracts are related to worse clinical outcomes in patients with cerebral autosomal-dominant arteriopathy with subcortical infarcts and leukoencephalopathy (CADASIL).[10] However, to date, the distribution patterns and longitudinal development of WMH in relation to rare *NOTCH3* variant carriers have not been described. Thus, studies on the spatial features of CSVD especially from longitudinal perspectives are required.

In addition to white matter lesions, brain atrophy also plays a significant role in the progression of CSVD.[11] Several studies have identified patterns of brain atrophy associated with both sporadic and Mendelian forms of CSVD,[12-14] highlighting its involvement in the disease process. However, quite a lot of studies did not observe the association,[15] possibly because of the complexities of their interactions, which are spatially and temporally heterogeneous, as well as differences between populations. Therefore, whether and how rare *NOTCH3* variants are related to brain atrophy and their interaction with WMH is crucial for a comprehensive characterization of their imaging features and potentially provides insights into the predictive clinical outcomes associated with these variants.

In a population-based sample, we aim to describe the spatial and dynamic patterns of CSVD in relation to rare *NOTCH3* variants from a longitudinal view and to investigate the interaction between regional cortical atrophy and white matter lesion progression.

Methods

Study Population

This study was part of the Shunyi study, an ongoing prospective community-based cohort study designed to investigate the risk factors and associated brain imaging of cardiovascular and age-related diseases. The design and methods of the Shunyi study have been described previously.[16] Between June 2013 and April 2016, all inhabitants aged 35 years and older living in Shunyi, a suburb district of Beijing, were invited. Baseline assessments, including structured questionnaires, physical examinations, and blood tests, were performed. We excluded those who had incomplete brain MRI or whole-exome sequencing (WES). After further excluding individuals with poor imaging quality for structural segmentation or CSVD assessment, we assembled the final cohort for baseline analysis. All participants were invited for a 5-year follow-up MRI, and those who fail to complete the follow-up brain MRI were excluded. After further excluding individuals with unsatisfying structural segmentation or lesion segmentation results, we assembled the final cohort for longitudinal analysis (the study flow diagram is provided in Figure 1). Separate quantification procedures were conducted for WMH lesion segmentations and surface-based anatomical segmentation results.

Standard Protocol Approvals, Registrations, and Patient Consents

All participants provided written informed consent. The study was approved by the Ethical Committee of Peking Union Medical College Hospital (reference number: B-160).

WES and Definition of Rare *NOTCH3* Variants

Quality control DNA samples and WES from 1,257 participants were subjected to high-depth WES. The protocol used for WES data assessment and quality control was provided in our previous publication.[5] In brief, *NOTCH3* variants with minor allele frequency <1% in all 4 public population databases were defined as rare variants, including 57 missense SNPs, of which 31 were located in epidermal growth factor-like repeats (EGFr).

Participants were first divided into 2 groups based on whether they carried a rare *NOTCH3* variant: the *NOTCH3*(+) group and the *NOTCH3*(−) group. The rare *NOTCH3* variant carriers were then divided into 2 subgroups based on whether the rare *NOTCH3* variant was located in EGFr, namely the EGFr(+) group and EGFr(−) group. The number of patients in each group is shown in the study flow diagram (Figure 1).

Figure 1 Study Flow Diagram

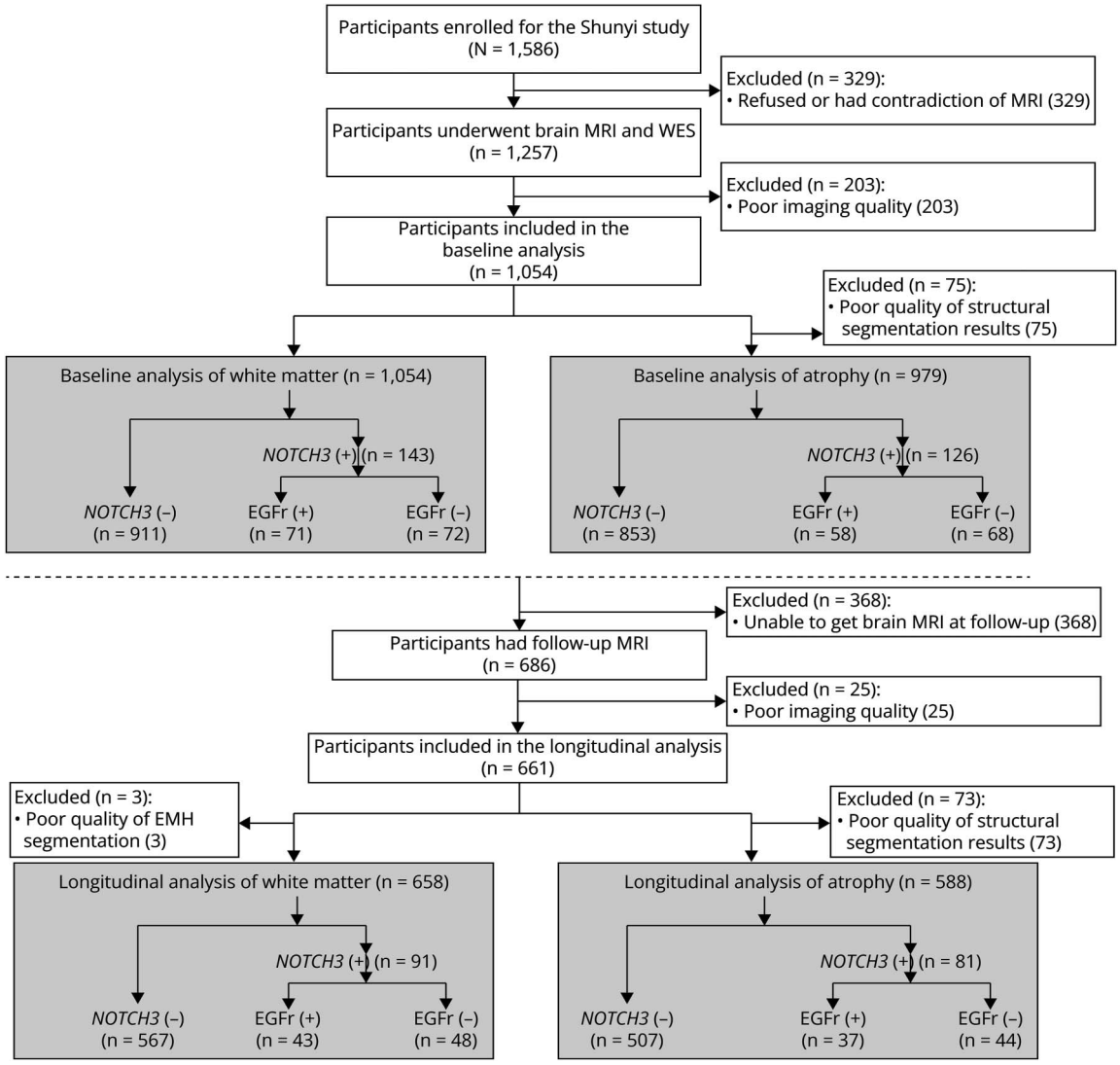

EGFr = epidermal growth factor-like repeat; WES = whole-exome sequencing; WMH = white matter hyperintensity.

Image Acquisition and Preprocessing

At baseline and follow-up, MRI was performed using the same scanner and protocols, and no scanner upgrades or other changes were made during the course of this study. The details of MRI acquisition have been described in our previous publications.[17] Three-dimensional (3D) T1-weighted, T2-weighted, and fluid-attenuated inversion recovery were performed as described in detail in the eMethods (links.lww.com/WNL/D137). We acquired 20 axial slices (thickness = 5 mm, gap = 1 mm) for fluid-attenuated inversion recovery images. We preprocessed the imaging data using the UK Biobank processing pipeline,[18] modified according to our MRI parameters.

Assessment of WMH

WMH Segmentation and Volumetric Measurement

We performed WMH segmentation at each time point using the brain intensity abnormality classification algorithm (BIANCA),[19] which is a fully automated method for classifying voxels based on relative intensity and spatial features. White matter hyperintensities were manually labeled on the FLAIR sequence in 25 participants as the training data. Both FLAIR and T1 images were used to train the segmentation algorithm using BIANCA. The BIANCA output consists of individual probability maps thresholded at 0.95 to produce a binary map of lesions (individual WMH map), where the individual WMH volume was extracted (mL). After the automated procedures, we conducted a visual inspection of the WMH masks generated by the segmentation algorithm in all participants. This manual review allowed us to assess the consistency of the automatically segmented masks with the original FLAIR images and make necessary corrections when required. This step was conducted to ensure the accuracy and completeness of lesion identification. Leave-one-out cross-validation[20] was used to assess the accuracy of the segmentation algorithm. Therefore, the dice

coefficient calculation of each manual labeled WMH mask did not overlap the training data used to build the automated label. The mean dice coefficient was 0.87 in our data set, and the interclass correlation coefficient was 0.94. The white matter hyperintensity volumes obtained were log-transformed because of their skewed distribution. The progression of WMH was calculated by subtracting the baseline volume from the follow-up volume, considering that the follow-up durations were balanced between the 2 groups.

Creating WMH Probability Maps

We produced group-wise WMH probability maps to display the spatial distribution of WMH lesions. To improve the comparability of WMH among individuals on the group level, we used linear (FLIRT)[21] and nonlinear alignment options (FNIRT[22] and applywarp) in FSL to align the FLAIR images to the Montreal Neurologic Institute (MNI) 152 standard space T1 template, and the transformation matrix was subsequently applied to the WMH mask to transform the WMH masks from native FLAIR space into MNI space. We used the trilinear interpolation method to register the mask edge into MNI space and rethresholded the mask at 0.5 to make it into a binary mask again which approximately preserves the size of the original mask. Subsequently, individual WMH masks were summed and divided by the number of subjects in the group, such that each voxel had the percentage of individuals who had WMH lesions at the specific voxel. For WMH progression maps, baseline individual non-WMH tissue masks were created by excluding the individual WMH mask from the whole-brain mask (both in MNI space). Second, individual WMH progression masks were calculated by masking follow-up WMH masks (in MNI space) with baseline non-WMH tissue masks. Third, individual WMH progression masks were summed and divided by the number of subjects in the group to create group-wise WMH progression maps, such that each voxel had the percentage of individuals who had new-onset WMH lesions at the specific voxel. WMH remission maps were also produced (details available in eMethods, links.lww.com/WNL/D137). We overlapped WMH maps on a standard brain to compare the different spatial patterns of WMH across variant groups.

Assessment of Atrophy Measures

Bias Correction and Quality Control

The following processing steps were performed to increase the reliability and statistical power: skull stripping, Talairach transforms, atlas registration, and parcellations using common information from the within-subject template. All segmentation and parcellation results were checked both visually and using the UK Biobank automatic quality check pipeline,[18] and those with poor quality were excluded.

Tissue Segmentation and Cortical Parcellation

After manually checking the quality of raw data, all images were processed using the following automatic segmentation pipeline. An automatic segmentation pipeline using Freesurfer image analysis suite v6.0 was performed in the native space, where structure volumes (gray matter and white matter) were extracted for global-wise analysis.[23] This approach allows for the preservation of subject-specific anatomical details. For longitudinal analysis, we also constructed a within-subject template (in native space) for each subject as an automatic surface reconstruction of different time points, where segmentation errors can be fixed.[24] Vertex-wise imaging cortical volume maps were obtained from the output of the stream stated above in the longitudinal FreeSurfer analysis suite. Therefore, we obtained a comprehensive description of cortical morphology for further vertex-wise analysis. Detailed methods of vertex-wise analysis are provided in the *Statistical image analysis*.

Definitions of Volumetric Measurements

To measure brain parenchymal atrophy, we calculated the brain parenchymal fraction (BPF) as the ratio of brain tissue volume (sum of gray matter and white matter volumes) to the TIV. The gray matter fraction (GMF) and white matter fraction (WMF) were calculated as the gray matter or white matter volume divided by the TIV. The annual change rates of the BPF, GMF, and WMF were calculated as the difference between the follow-up and baseline values divided by the follow-up interval (years).

Assessment of Lacunes and CMBs

The definitions of lacunes and cerebral microbleeds (CMBs) at baseline were previously described by Zhai et al.[17] Lacunes and CMBs were each rated by a single neurologist (trained specifically to read lacunes/CMBs) who was blinded to clinical data (FH for lacunes and QW for CMBs). In uncertain cases, the group consensus was determined. In brief, lacunes were defined as focal fluid intensity cavities of 3–15 mm in diameter located in the basal ganglia, subcortical white matter, or brain stem. CMBs were defined as small, round-shaped, hypointense lesions on susceptibility-weighted imaging.[25] The intra-rater agreements were 0.95 for lacunes and 0.90 for CMBs.

New-onset lacunes and CMBs were also defined as dichotomous variables, and the definition of their presence followed the same protocols with a baseline assessment, rated by 2 trained physicians (SMJ for lacunes and TMY for CMBs) who were blinded to all clinical data. Lacunes/CMBs at baseline and follow-up brain images were evaluated independently. In cases where the evaluator was uncertain about the diagnosis of the lesion, baseline and follow-up scans were directly compared, and a group consensus was reached. New-onset lacunes or CMBs were defined as any condition of the following 2: (1) zero lesion at baseline and at least one lesion at follow-up; (2) the same number of lesions at baseline and follow-up, but at different locations.

Assessment of Other Baseline Characteristics

Demographic and clinical information, including age, sex, blood pressure, hypertension, diabetes mellitus, hyperlipidemia, smoking history, and current medication, was collected using a

Table 1 Characteristics of the Study Population

Variable	Mean (SD) or N (%)				t or χ^{2a}	p Value[a]	t or χ^{2b}	p Value[b]	t or χ^{2c}	p Value[c]
	All	*NOTCH3*(−)	*NOTCH3*(+)							
			EGFr(+)	EGFr(−)						
Baseline demographics										
No. participants at baseline	1,054	911	71	72	—	—	—	—	—	—
Age, y	57.18 (9.36)	57.14 (9.28)	57.99 (9.68)	56.89 (10.10)	−0.340	0.731	−0.730	0.463	0.220	0.824
Male, n (%)	380 (36.05)	323 (35.46)	30 (42.25)	27 (37.5)	1.040	0.308	1.322	0.250	0.122	0.727
Diabetes mellitus, n (%)	174 (16.51)	146 (16.03)	16 (22.54)	12 (16.67)	1.133	0.287	2.026	0.155	0.020	0.887
Hypertension, n (%)	543 (51.52)	469 (51.48)	38 (53.52)	36 (50.00)	0.004	0.953	0.110	0.741	0.059	0.809
Hyperlipidemia, n (%)	501 (47.53)	434 (47.64)	30 (42.25)	37 (51.39)	0.031	0.861	0.767	0.381	0.376	0.540
Current smoker, n (%)	244 (23.15)	202 (22.17)	22 (30.99)	20 (27.78)	3.599	0.058	2.905	0.088	1.199	0.274
Stroke history, n (%)	38 (3.62)	28 (3.08)	8 (11.43)	2 (2.78)	5.517	0.019[d]	12.765	<0.001[d]	0.021	0.885
Baseline brain structural parameters										
WMH volume, median (IQR), mL	0.94 (0.27–3.00)	0.85 (0.26–2.86)	1.70 (0.37–4.98)	1.52 (0.28–3.1)	−2.270	0.025[d]	−2.440	0.017	−0.730	0.465
Presence of CMB, n (%)	116 (11.01)	98 (10.76)	11 (15.49)	7 (9.72)	0.423	0.516	1.497	0.221	0.075	0.784
Presence of lacune, n (%)	169 (16.05)	157 (17.68)	20 (28.57)	14 (20.59)	0.007	0.010[d]	0.003	0.006[d]	0.294	0.305
White matter fraction	0.32 (0.02)	0.32 (0.02)	0.32 (0.02)	0.32 (0.02)	2.010	0.045[d]	0.670	0.505	2.210	0.028
Gray matter fraction	0.41 (0.02)	0.41 (0.02)	0.41 (0.02)	0.41 (0.02)	−0.220	0.829	0.180	0.861	−0.460	0.644
Brain parenchyma fraction	0.75 (0.03)	0.75 (0.03)	0.75 (0.03)	0.75 (0.03)	1.360	0.175	0.690	0.493	1.270	0.204
Longitudinal changes of brain structural parameters										
No. of participants with follow-up MRI	661	570	43	48	—	—	—	—		—
Follow-up duration, y	5.53 (0.48)	5.53 (0.47)	5.657 (0.461)	5.474 (0.489)	−0.620	0.539	−1.730	0.084	0.750	0.454
WMH volume change, mL	2.46 (3.356)	2.455 (3.347)	2.43 (2.677)	2.565 (4.149)	−0.100	0.918	−0.170	0.866	0.050	0.961
Brain parenchyma fraction annual change, $\times 10^{-3}$/y	−0.283 (0.187)	−0.286 (0.188)	−0.274 (0.192)	−0.255 (0.174)	0.780	0.326	0.200	0.719	0.910	0.295
Gray matter fraction annual change, $\times 10^{-3}$/y	−0.167 (0.124)	−0.17 (0.125)	−0.145 (0.113)	−0.151 (0.116)	1.380	0.152	1.040	0.254	0.970	0.338
White matter fraction annual change, $\times 10^{-3}$/y	−0.112 (0.113)	−0.112 (0.109)	−0.128 (0.144)	−0.099 (0.126)	−0.170	0.976	−0.750	0.506	0.590	0.463
Presence of new CMBs, n (%)	48 (7.26)	41 (7.19)	3 (6.98)	4 (8.33)	0.029	0.865	0.003	0.958	0.085	0.770
Presence of new lacune, n (%)	71 (10.74)	62 (10.88)	4 (9.30)	5 (10.42)	0.080	0.778	0.103	0.748	0.010	0.922
New-onset stroke	45 (4.27)	39 (4.28)	4 (5.63)	2 (2.78)	0.002	0.963	0.288	0.544	0.377	0.762

Abbreviations: CMBs = cerebral microbleeds; EGFr = epidermal growth factor–like repeat; WMH = white matter hyperintensity.
Data represent mean (SD), median (IQR), or frequency (percentage). Significance tests between the groups were performed using the χ^2 test or two-sample t test.
[a] Significance test between the *NOTCH3*(+) group and *NOTCH3*(−) group.
[b] Significance test between the EGFr(+) group and *NOTCH3*(−) group.
[c] Significance test between the EGFr(−) group and *NOTCH3*(−) group.
[d] Surviving a false discovery rate (FDR)–corrected threshold of P(FDR) = 0.05.

Table 2 Rare *NOTCH3* Variants and White Matter Hyperintensity Burden

	Baseline WMH volume			WMH volume change[a]		
	β	95% CI	*p*	β	95% CI	*p*
***NOTCH3*(+) vs *NOTCH3*(−), n = 143 and n = 911**						
Model 1	0.169	0.053 to 0.285	0.004[b]	0.073	−0.158 to 0.303	0.536
Model 2	0.162	0.047 to 0.276	0.006[b]	0.046	−0.185 to 0.277	0.695
EGFr-involving vs *NOTCH3*(−), n = 71 and n = 911						
Model 1	0.263	0.103 to 0.422	0.001[b]	0.025	−0.304 to 0.355	0.880
Model 2	0.247	0.090 to 0.405	0.002[b]	−0.030	−0.363 to 0.303	0.859
EGFr-sparing vs *NOTCH3*(−), n = 72 and n = 911						
Model 1	0.078	−0.078 to 0.233	0.326	0.117	−0.190 to 0.424	0.455
Model 2	0.081	−0.073 to 0.234	0.302	0.125	−0.182 to 0.433	0.423

Abbreviations: EGFr = epidermal growth factor–like repeat; WMH = white matter hyperintensity.
Model 1 is adjusted for age, sex, TIV, and BPF change rate; model 2 is adjusted for age, sex, TIV, BPF change rate, follow-up interval, and cardiovascular risk factors (hypertension, diabetes, hyperlipidemia, and any smoking history.
[a] WMH volume change was calculated by subtracting the baseline volume from the follow-up volume (log-transformed).
[b] Surviving a false discovery rate (FDR)–corrected threshold of P(FDR) = 0.05.

structured questionnaire and physical examination. Definitions of cardiovascular risk factors are provided in eMethods, links.lww.com/WNL/D137).

Statistical Global Data Analysis

For the description of characteristics of the overall and group-wise population, continuous variables were expressed as mean with SD or median with interquartile range (IQR), and categorical variables were expressed as frequencies and proportions. We compared the baseline characteristics of participants with and without rare *NOTCH3* variants using univariate analysis. For analysis of subgroups of rare *NOTCH3* variant locations, we compared global measures in EGFr(+) vs *NOTCH3*(−) groups and EGFr(−) vs *NOTCH3*(−) groups. We corrected for multiple testing in the 2 models using false discovery rate (FDR) correction using the Benjamini-Hochberg method.[26] All statistical analyses were conducted using SAS 9.4. Statistical significance was set at $p < 0.05$ by FDR correction.

The relationships of rare *NOTCH3* variants with global cortical and white matter measures were examined using general linear models (linear regression and logistic regression), with CSVD measurement as the determinant and rare *NOTCH3* variant status as the dependent variable. Two models were used for adjusting confounding factors in a stepwise manner. Model 1 is adjusted for age and sex; model 2 is additionally adjusted for age, sex, and cardiovascular risk factors (hypertension, diabetes, hyperlipidemia, and any smoking history). Follow-up interval, TIV, and BPF change rate were also adjusted in the 2 models regarding the analysis of WMH volumes. The assumptions of the above models were checked using residual diagnosis plots.

To determine the effect of the presence of rare *NOTCH3* variants on new-onset lacunes and CMBs, we employed logistic regression with lesion presence as a determinant and variant groups as dependent variables, using the above 2 models.

Statistical Image Analysis

Voxel-Base Analysis of WMH

A general linear model analysis was performed using a permutation-based statistical interference tool for a non-parametric approach ('randomize') using FSL.[18] For cross-sectional analysis, the individual probability maps produced by BIANCA were masked by individual WMH masks and merged into a single 4D image file and fed into the voxel-wise statistics, thereby avoiding false-positive discovery in voxels that were not considered as WMH. For the longitudinal analysis, a linear fit was calculated with respect to the scan interval to generate WMH progression rate maps for each subject (individual WMH progression rate maps). Individual WMH progression rate maps were then normalized to MNI space (standard WMH progression rate maps), merged into a single 4D image file, and fed into the voxel-wise statistics such that the difference in WMH distribution would be examined on a group level. The number of permutation tests was 5,000, and the threshold for significance was threshold-free cluster enhancement[19,27] corrected at $p < 0.05$, adjusted for age, sex, and cardiovascular risk factors (hypertension, diabetes, hyperlipidemia, and any smoking history.

Vertex-wise Analysis of the Cortex

A hypothesis-free vertex-wise general linear model approach of the entire cortex was applied to evaluate the relationship between the variant groups and cortical volume using mri_glmfit in FreeSurfer. Two-stage models were applied for longitudinal

Figure 2 Rare NOTCH3 Variants and Aging-Related Alterations of White Matter Hyperintensity Volume and Brain Parenchymal Fraction

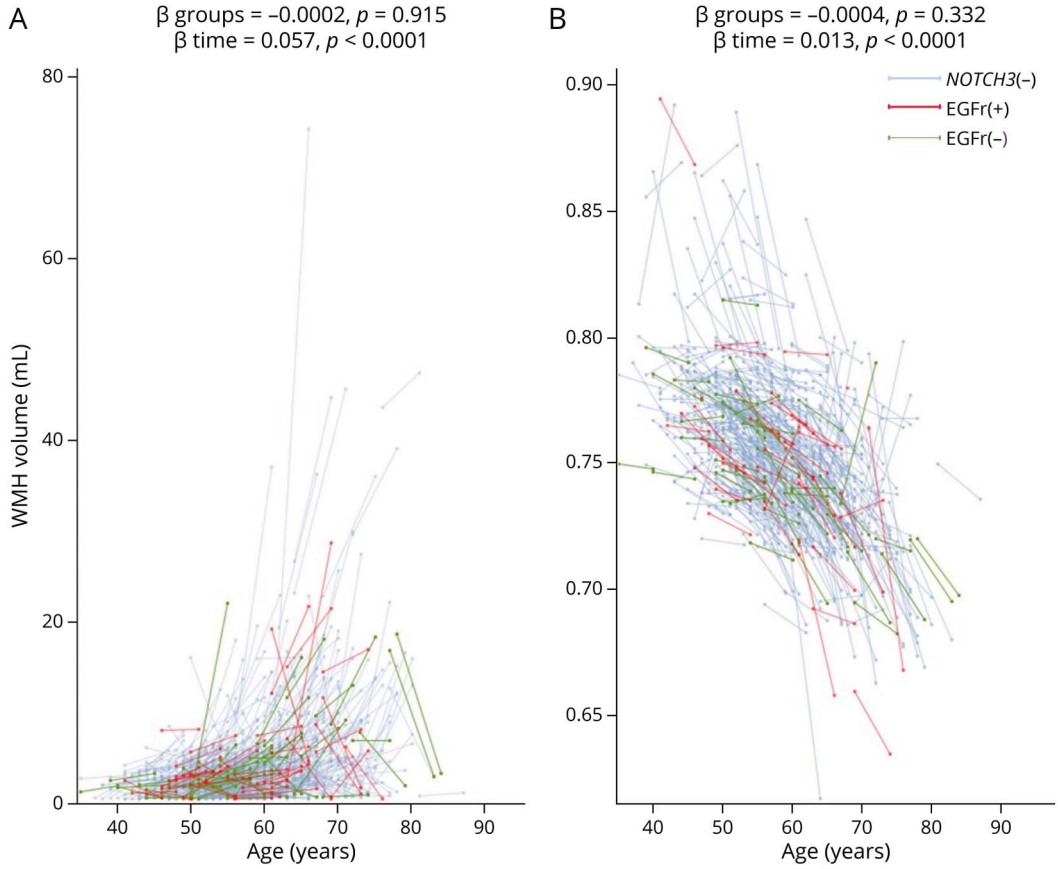

(A) The left plot depicts the dynamic change in white matter hyperintensity volume (WMH) volume (mL) over the follow-up period along with age at the individual level and stratified by variant groups. (B) The dynamic change in brain parenchymal fraction (BPF) stratified by variant groups. β groups denote the estimated effect of age*group interaction in the linear fit of longitudinal change; β time denotes the estimated change in WMH volume or BPF for every 1-year increase in age.

analysis, where the percent change in the vertex-wise maps was calculated with respect to the scan interval. Furthermore, we explored the relationship between the WMH volume change rate and atrophy by applying a vertex-wise general linear model. All general linear models were controlled for age and sex. Significant clusters were determined by the permutation method (permutation number = 5,000) at a cluster-corrected level of $p < 0.05$ (cluster-forming vertex threshold was set at $p < 0.001$) across both hemispheres.

Data Availability

On request from qualified investigators, anonymized data will be shared solely for the purpose of replicating the procedures and results presented in the article, after obtaining ethics clearance and approval from all members of the project group.

Results

Demographics

Finally, 1054 participants were included in the baseline analysis of WMH, lacunes, and CMBs, and 979 participants were included in the baseline analysis of brain volumes. For longitudinal analysis, 661 participants remained in the final cohort. The baseline and longitudinal characteristics are presented in Table 1. Of the 1,054 participants included at baseline (mean age 57.18 ± 9.36 years, 36.05% men), 13.56% (143/1,054) were carriers of rare *NOTCH3* variant, and 6.73% (71/1,054) were EGFr-involving variants. A total of 661 (62.7%) participants underwent brain MRI follow-up for a mean interval of 5.53 ± 0.48 years. Among them, 13.76% (91/661) carried rare *NOTCH3* variants and 6.51% (43/661) were EGFr-involving variants. Those lost to MRI follow-up were significantly older and had a higher prevalence of cardiovascular risk factors and heavier baseline CSVD burden than followed participants (eTable 1, links.lww.com/WNL/D137).

Overall Image Characteristics

Overall, the white matter lesions and brain atrophy progressed throughout the study period (Table 1). For WMH, the median (IQR) volume was 0.94 (0.27–3.00) mL at baseline, and the mean (SD) progress was 2.46 ± 3.36 mL. The presence of lacunes or CMBs was observed in 16.03%

Figure 3 Rare *NOTCH3* Variants and Spatial Patterns of WMH

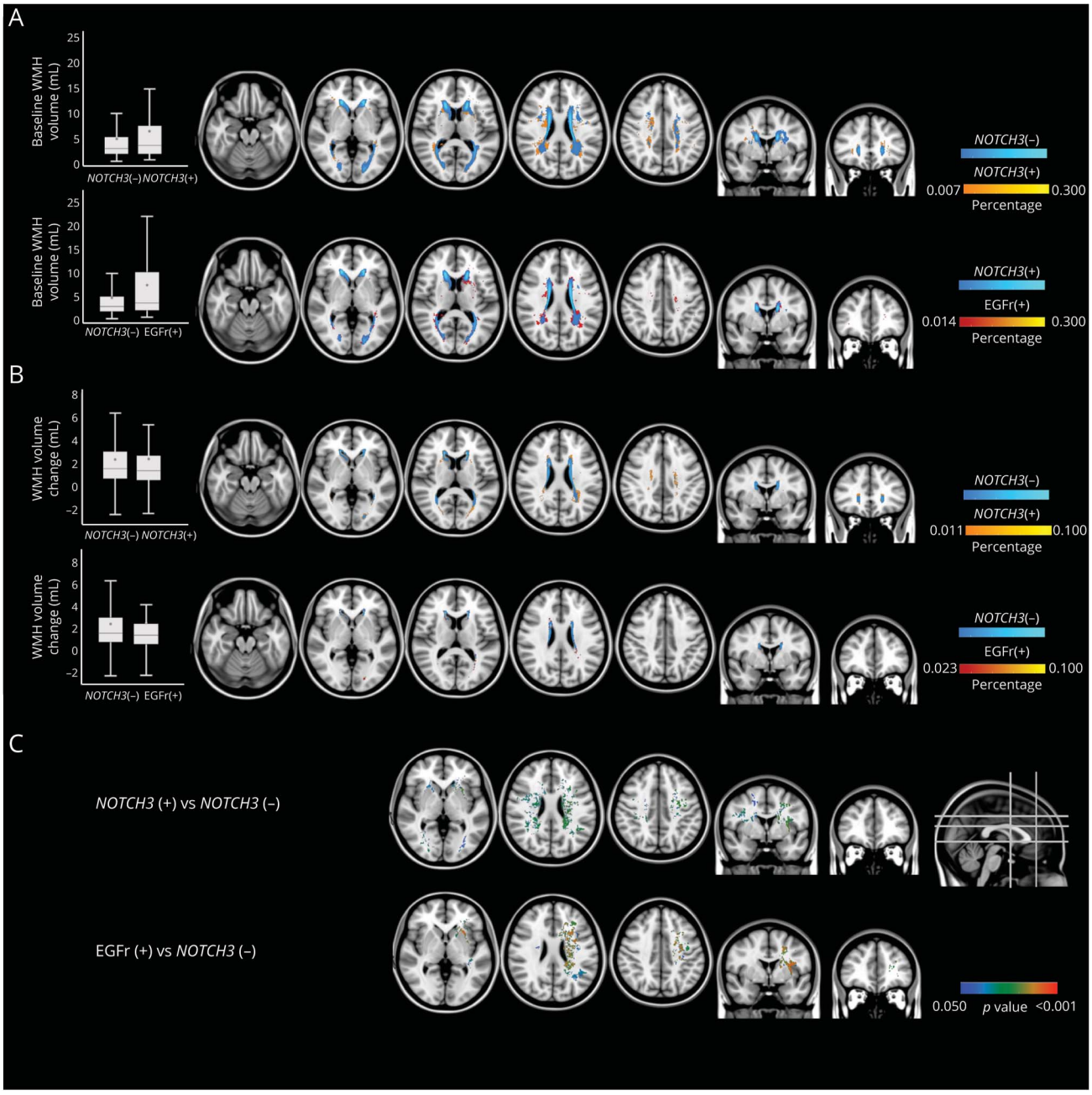

(A) The distribution of baseline WMH in different variant groups, and (B) the distribution of WMH progression in different variant groups. The total volumes of baseline WMH or WMH progression in different groups were shown as a box plot on the left. Brain slices show the average WMH probability map for the *NOTCH3*(+) group (yellow scale, upper panel) or the EGFr(+) group (red scale, lower panel) on top of that of the *NOTCH3*(−) group (blue scale). The threshold for the *NOTCH3*(+) group is set at 0.007 to 0.3 in baseline maps and 0.011 to 0.1 in progression maps while for the EGFr(+) group, it is set at 0.014 to 0.3 in baseline maps and 0.023 to 0.1 in progression maps. The percentage of participants who had WMH in a particular voxel is depicted in the color bar. (C) The significant clusters where the baseline WMH is positively related to rare *NOTCH3* variants (upper panel) or EGFr-involving variants (lower panel) (threshold-free cluster enhancement corrected $p < 0.05$, adjusted for age, sex, hypertension, diabetes, hyperlipidemia, and any smoking history). The p values of correlation tests between the variant status and probability of WMH in a particular voxel are depicted in the red-blue color bar. No significant clusters were found comparing WMH progression rate maps between variant groups. EGFr = epidermal growth factor-like repeat; WMH = white matter hyperintensities.

(169/1,054) and 11.01% (116/1,054) of participants at baseline, respectively, while 10.74% (71/661) and 7.26% (48/661) had new-onset lacunes and CMBs at follow-up, respectively. The average BPF at baseline was 0.75 ± 0.03, with a mean (SD) annual change of $-0.283 \pm 0.187 \times 10^{-3}$/year. The WMH progression was strongly correlated with the BPF change rate (Pearson R = −0.27, $p < 0.0001$, adjusted for age and sex). In all followed participants, WMH lesions and brain parenchymal atrophy were severer along with age, and older patients had steeper BPF decreases over time.

Table 3 Rare *NOTCH3* Variants and Brain Atrophy

	Baseline BPF			BPF change[a]		
	β	95% CI	*p*	β	95% CI	*p*
***NOTCH3*(+) vs *NOTCH3*(−), n = 143 and n = 911**						
Model 1	−0.004	−0.008 to 0.000	0.057	0.025	−0.015 to 0.065	0.213
Model 2	−0.004	−0.008 to 0.000	0.077	0.031	−0.008 to 0.071	0.115
EGFr-involving vs *NOTCH3*(−), n = 71 and n = 911						
Model 1	−0.003	−0.009 to 0.003	0.303	0.021	−0.036 to 0.078	0.473
Model 2	−0.003	−0.009 to 0.003	0.407	0.034	−0.023 to 0.090	0.241
EGFr-sparing vs *NOTCH3*(−), n = 72 and n = 911						
Model 1	−0.005	−0.011 to 0.001	0.081	0.029	−0.024 to 0.081	0.285
Model 2	−0.005	−0.010 to 0.001	0.080	0.030	−0.022 to 0.081	0.258

Abbreviations: BPF = brain parenchymal fraction; EGFr = epidermal growth factor–like repeat.
Model 1 is adjusted for age and sex; Model 2 is adjusted for age, sex, and cardiovascular risk factors (hypertension, diabetes, hyperlipidemia, and any smoking history).
[a] BPF change was calculated as the difference between the follow-up and baseline values divided by the follow-up interval (y).

We also observed remission of WMH over the follow-up period. Of the 24 (3.63%) participants with decreased WMH volume at follow-up, the median (IQR) of WMH volume change was −0.77(−1.74 to −0.41) mL. Among them, 3 participants had rare *NOTCH3* variants while only one had an EGFr-involving variant. Extra details are demonstrated in the eResults and eFigures 1 and 2 (links.lww.com/WNL/D137).

Rare *NOTCH3* Variants and WMH Distribution Patterns

Global WMH Burden

Compared with noncarriers, participants with rare *NOTCH3* variants had larger WMH volumes (1.65 vs 0.85 mL, p = 0.025) (Table 1). The differences were also significant between the EGFr(+) and *NOTCH3*(−) groups.

A a stable association between rare *NOTCH3* variants and baseline WMH volumes is shown in Table 2 (β [95% CI] = 0.162 [0.047–0.276], p = 0.006, independent of age, sex, TIV, BPF change rate, and cardiovascular risk factors). In the longitudinal analysis, we found no difference in WMH progression among *NOTCH3* variant groups.

To illustrate the age-related effects of the rare *NOTCH3* variant on the dynamic profile of WMH progression, we performed WMH volume plotting with age at the individual level over the follow-up period and stratified by variant groups (Figure 2A). We found that both carriers and noncarriers had faster WMH progression along with older age while we found an interaction between variant groups and age was not significant.

WMH Distribution Pattern

Figure 3 shows the spatial distribution of baseline and new-onset WMH. As shown in lesion probability maps (Figure 3A), the WMH of participants with rare *NOTCH3* variants (especially EGFr-involving variants) was more extensive compared with that of noncarriers, involving the bilateral pyramidal tracts and superior thalamic radiation. The spatial distribution of new-onset WMH was also more extensive in rare *NOTCH3* variants carriers (Figure 3B) while the progression region in all groups was mostly confined to periventricular caps and thin lining along the lateral ventricles.

We also compared the distribution of WMH among the variant groups via voxel-wise generalized linear model (GLM) analysis (Figure 3C) and found that rare *NOTCH3* variant carriers had a higher probability of WMH presence at baseline in multiple regions, which were predominantly located in periventricular areas with several small clusters scattered in the deep white matter (threshold-free cluster enhancement corrected p-value <0.05, adjusted for age and sex). No significant clusters were identified by comparing the WMH progression rate maps among the variant groups.

Rare *NOTCH3* Variants and Atrophy Patterns

Global Brain Parenchyma Atrophy

As shown in Table 3, carriers of rare *NOTCH3* variants had a lower baseline BPF than noncarriers (β = −0.004, SE = 0.002, p = 0.057, adjusted for age and sex), although the difference was not statistically significant. In the longitudinal analysis, we observed no difference in atrophy progression speed among *NOTCH3* variant groups, after adjusting for age and sex.

The dynamic profile of BPF progression during the follow-up period in the different *NOTCH3* variant groups is shown in Figure 2B. We observed a lower BPF and faster BPF shrinking at an older age, but this trend did not differ among the variant groups.

Figure 4 Rare *NOTCH3* Variants and Spatial Patterns of Cortical Atrophy

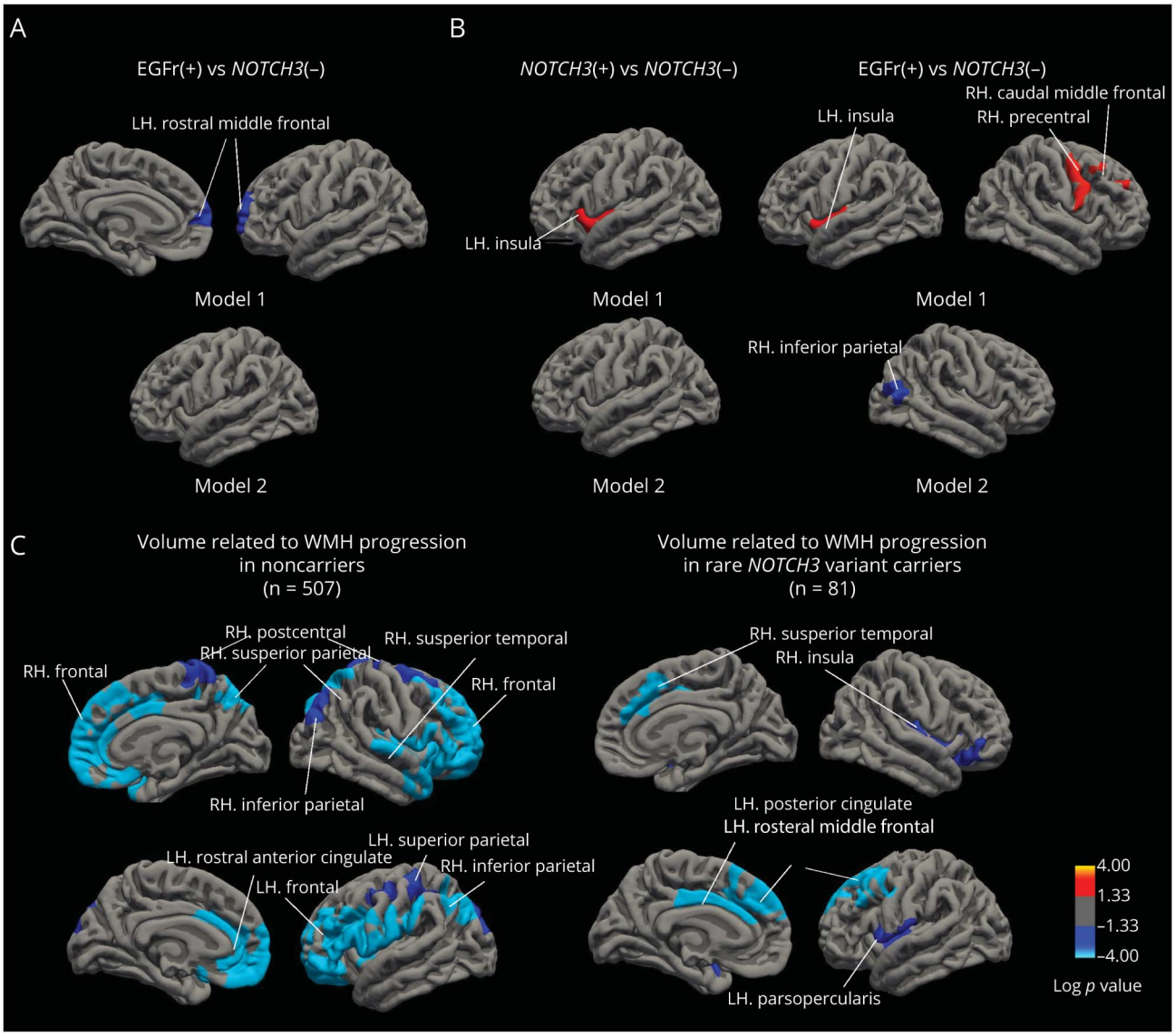

(A) The baseline cortex volume map related to EGFr-involving variant status. (B) The cortex volume rate map related to the *NOTCH3* variant of EGFr-involving variant status, in raw models (model 1) and adjusted models for age and sex (model 2). (C) Significant clusters of cortex volume rate map related to the progression of WMH volume, in the *NOTCH3* (–) group and the *NOTCH3* (–) group, respectively (adjusted for age and sex). The color scale at the bottom represents the statistical significance of a positive or negative relationship (cluster-wise *p*-value <0.05, multicomparison corrected). Significant clusters were labeled according to the Desikan-Killiany atlas. EGFr = epidermal growth factor-like repeat; WMH = white matter hyperintensities.

Atrophy Distribution Pattern

In the vertex-wise analysis of the baseline cortical volume, we found that EGFr-involving variants were related to a smaller volume of clusters in the frontal lobe (cluster-wise $p < 0.05$, multiple comparison corrected) while the significance disappeared after adjustment for age and sex (Figure 4A). Detailed information on significant clusters, including MNI coordinates, size, and statistics, is provided in eTable 2 (links.lww.com/WNL/D137). No significant cluster was identified in the comparison of *NOTCH3*(+) vs *NOTCH3*(–) groups.

For longitudinal analysis, we detected widespread shrinkage of the cortex volume among both carriers and noncarriers of rare *NOTCH3* variants (eFigure 3, links.lww.com/WNL/D137). However, in the longitudinal GLM analysis, no significant clusters were identified in the comparison of the *NOTCH3*(+) vs *NOTCH3*(–) groups while only a small cluster in the inferior parietal lobe was identified with faster volume reduction in the EGRr(+) group than in the *NOTCH3*(–) group (cluster-wise $p < 0.05$, multiple comparison corrected, adjusted for age and sex) (Figure 4B).

Cortical Atrophy Related to WMH Progression

The WMH progression was strongly correlated with the BPF change rate in rare *NOTCH3* variants (Pearson R = –0.512, $p < 0.0001$) and noncarriers (Pearson R = –0.164, $p = 0.0002$)

after adjusting for age and sex. As shown in Figure 4C, among the carriers of rare *NOTCH3* variants, cortical atrophy of multiple regions in the frontal and parietal lobes was related to the WMH progression (cluster-wise $p < 0.05$, multiple comparison corrected, adjusted for age and sex). The corresponding relationships among the noncarriers showed similar spatial patterns.

In the baseline population, 38/1,054 participants had a stroke history while 45 of 661 participants had a new-onset stroke during follow-up. Analysis of rare NOTCH3 variants and imaging characteristics in participants without stroke are available in the eTable 3 (links.lww.com/WNL/D137).

Rare *NOTCH3* Variants and Lacunes/CMBs

The results of this part are available in the eResults, eTables 4–6 (links.lww.com/WNL/D137).

Discussion

In this longitudinal study, we observed a more severe pattern of brain parenchymal damage in participants with rare *NOTCH3* variants. These variant carriers showed susceptibility to a heavier global CSVD burden and, more importantly, had more extensive WMH distributed in the periventricular areas. These features appeared to be more prominent in the EGFr-involving subgroup. In addition, we observed worse cortical atrophy in EGFr-involving rare *NOTCH3* variant carriers, and the progression of frontal brain atrophy is related to WMH progression.

Our findings of heavier global WMH burden associated with rare *NOTCH3* variants are consistent with our previous work[5] and the earlier report of Schmidt[6] in a population-based cohort and the report of Ramirez[28] in patients with Parkinson disease. In addition, this association appeared more prominent in EGFr-involving variants. EGFr encodes the main extracellular domain of the *NOTCH3* protein, and it is also involved in ligand binding and glycosylation. *NOTCH3* cysteine-sparing variants on EGFr, which lead to an odd number of cysteine residues, are well-known as typical genetic pathogenesis of CADASIL. Based on current research findings, it is speculated that this might be the only pathogenic pathway for *NOTCH3* variants. Rare *NOTCH3* variants involving EGFr may promote the occurrence and development of CSVD through other mechanisms, including abnormal regulation of *NOTCH3* O-glycosylation[29] and loss of the beta-sheet structure,[26,30] resulting in impaired function of the notch3 protein. Therefore, *NOTCH3*-related CSVD may represent a broad disease spectrum, with CADASIL contributing to an extreme phenotype within this spectrum. Thus, it is understandable that most participants in our cohort had less burden than typical CADASIL patients, which is inconsistent with the classical distribution of lesions. Considering the effect of multiple rare missense *NOTCH3* SNPs pooled in this analysis, further studies on specific sites of *NOTCH3* cysteine-sparing variants are needed to explore their pathogenic pathways and association with CSVD severity.

The dynamic features of CSVD in rare *NOTCH3* variant carriers were also described in this study. In this middle-aged elderly population, we did not discover a faster deterioration of WMH in those with rare *NOTCH3* variants during the 5-year follow-up period, although they had a heavier burden at baseline. This implies that WMH in rare *NOTCH3* variant carriers might already accumulate before middle age, and the accumulating speed might not be distinguishably high in a 5-year follow-up in middle age. Whether this genetic predisposition had a steady effect during the life span or might be more significant under certain environmental factors need further investigation.

To achieve a deeper recognition of imaging characteristics beyond global burden measurement, this study provided a profile of the spatial distribution of WMH in rare *NOTCH3* variant carriers. The distribution and progression regions of WMH in *NOTCH3* variant carriers overlap with the locations of WMH related to sporadic SVD but are more extensive, predominantly involving the condensed long tracts such as pyramidal tracts and superior thalamic radiation. In addition, WMH in these regions has widespread functional correlation (cognition and motor functions) of white matter tracts architecture in the periventricular region.[8,10,31,32] Therefore, WMH in *NOTCH3* variant carriers is likely to result in neurologic deficit symptoms such as gait disorders and cognitive decline; however, our hypothesis requires further validation in future research.

Over the follow-up period, we observed that participants with rare *NOTCH3* variants had widespread cortical atrophy. More interestingly, we proposed a phenotypic pattern of cortical atrophy related to WMH progression independent of age. Although brain atrophy has been listed as an imaging marker of CSVD, its relationship with white matter lesions is still a topic of discussion. Notably, several large studies have reported controversial results,[15] as variability exists in population characteristics, disease stage, and processing methods. Nevertheless, our findings add to evidence of brain atrophy interacting with white matter lesions in *NOTCH3* variant carriers because the atrophic regions related to WMH progression met the projection areas of periventricular white matter tracts.

The strengths of this study include a large sample size, a population-based design cohort with a long follow-up duration, and comprehensive high-quality clinical, MRI, and WES data. Moreover, quantitative CSVD measurements were obtained by automatic segmentation with manual quantification, achieving a spatial description of lesions and reducing the risk of information bias. In addition, this study described the spatial pattern of CSVD in rare *NOTCH3* variant carriers based on voxel-based WMH maps and vertex-wise cortical morphology, manual quantification, and within-subject correction across different time points.

This study had some limitations. First, the long-interval follow-up design introduces attrition bias, and the progression of CSVD would probably be underestimated because those

who dropped out were older and had a heavier CSVD burden. Second, the image processing may have distorted the shape of WMH lesions, potentially leading to the loss of certain spatial features. Third, comparisons between carriers and noncarriers of rare *NOTCH3* variants involved heterogeneous and cumulative effects of all rare variants in the *NOTCH3* gene. As individual variants had a low incidence in the present population, their independent effects should be analyzed in a larger sample. In addition, lacunes and CMB are less frequent compared with WMH, leading to potential underpowering of the analysis related to these lesions. Fourth, the 2D MRI flair image (thickness = 5 mm, gap = 1 mm) was used for WMH segmentation, thus small longitudinal changes might be missed because of the different head positions of the two time points. Finally, this study did not report any neuropsychological or motor measures. Nevertheless, we have formally performed neuropsychological battery and quantitative gait measurements and shall analyze their correlation with rare *NOTCH3* variants in our future work.

In conclusion, we demonstrated a distinct pattern of brain parenchymal damage related to CSVD in participants with rare *NOTCH3* variants. Our findings indicated that individuals with rare *NOTCH3* variants should be regarded as a population susceptible to CSVD. Further studies in more populations are required to investigate the reproducibility of our findings and the underlying pathogenic mechanisms.

Study Funding

National Natural Science Foundation of China (No. 81971138), the Chinese Academy of Medical Sciences (CAMS) Innovation Fund for Medical Sciences (CIFMS) (CIFMS 2021-I2M-C&T-B-012), and the Strategic Priority Research Program "Biological basis of aging and therapeutic strategies" of the Chinese Academy of Sciences (grant XDB39040300).

Disclosure

The authors report no relevant disclosures. Go to Neurology.org/N for full disclosures.

Publication History

Received by *Neurology* June 12, 2023. Accepted in final form August 10, 2023. Submitted and externally peer reviewed. The handling editor was Editor-in-Chief José Merino, MD, MPhil, FAAN.

Appendix Authors

Name	Location	Contribution
Zi-Yue Liu, MD	Department of Neurology, State Key Laboratory of Complex Severe and Rare Diseases, Peking Union Medical College Hospital, Chinese Academy of Medical Sciences and Peking Union Medical College, Beijing, China	Drafting/revision of the manuscript for content, including medical writing for content; drafting/revision of the manuscript for content, including medical writing for content; major role in the acquisition of data
Fei-Fei Zhai, MD	Department of Neurology, State Key Laboratory of Complex Severe and Rare Diseases, Peking Union Medical College Hospital, Chinese Academy of Medical Sciences and Peking Union Medical College, Beijing, China	Drafting/revision of the manuscript for content, including medical writing for content; major role in the acquisition of data; analysis or interpretation of data
Jing-Yi Liu, MD	Department of Radiology, State Key Laboratory of Complex Severe and Rare Diseases, Peking Union Medical College Hospital, Chinese Academy of Medical Sciences and Peking Union Medical College, Beijing, China	Drafting/revision of the manuscript for content, including medical writing for content; major role in the acquisition of data; analysis or interpretation of data
Yi-Jun Zhou, MD	Department of Radiology, State Key Laboratory of Complex Severe and Rare Diseases, Peking Union Medical College Hospital, Chinese Academy of Medical Sciences and Peking Union Medical College, Beijing, China	Drafting/revision of the manuscript for content, including medical writing for content; major role in the acquisition of data; analysis or interpretation of data
Mei-Jun Shu, MD	Department of Neurology, State Key Laboratory of Complex Severe and Rare Diseases, Peking Union Medical College Hospital, Chinese Academy of Medical Sciences and Peking Union Medical College, Beijing, China	Drafting/revision of the manuscript for content, including medical writing for content; major role in the acquisition of data; analysis or interpretation of data
Xiao-Hong Huang, MD	Department of Neurology, State Key Laboratory of Complex Severe and Rare Diseases, Peking Union Medical College Hospital, Chinese Academy of Medical Sciences and Peking Union Medical College, Beijing, China	Drafting/revision of the manuscript for content, including medical writing for content; major role in the acquisition of data; analysis or interpretation of data
Fei Han, MD	Department of Neurology, State Key Laboratory of Complex Severe and Rare Diseases, Peking Union Medical College Hospital, Chinese Academy of Medical Sciences and Peking Union Medical College, Beijing, China	Major role in the acquisition of data; study concept or design
Ming-Li Li, MD	Department of Radiology, State Key Laboratory of Complex Severe and Rare Diseases, Peking Union Medical College Hospital, Chinese Academy of Medical Sciences and Peking Union Medical College, Beijing, China	Study concept or design
Li-Xin Zhou, MD	Department of Neurology, State Key Laboratory of Complex Severe and Rare Diseases, Peking Union Medical College Hospital, Chinese Academy of Medical Sciences and Peking Union Medical College, Beijing, China	Major role in the acquisition of data; study concept or design

Appendix *(continued)*

Name	Location	Contribution
Jun Ni, MD, PhD	Department of Neurology, State Key Laboratory of Complex Severe and Rare Diseases, Peking Union Medical College Hospital, Chinese Academy of Medical Sciences and Peking Union Medical College, Beijing, China	Major role in the acquisition of data; study concept or design
Ming Yao, MD	Department of Neurology, State Key Laboratory of Complex Severe and Rare Diseases, Peking Union Medical College Hospital, Chinese Academy of Medical Sciences and Peking Union Medical College, Beijing, China	Major role in the acquisition of data; study concept or design
Shu-Yang Zhang, MD, PhD	Department of Cardiology, State Key Laboratory of Complex Severe and Rare Diseases, Peking Union Medical College Hospital, Chinese Academy of Medical Sciences and Peking Union Medical College	Study concept or design
Li-Ying Cui, MD, PhD	Department of Neurology, State Key Laboratory of Complex Severe and Rare Diseases, Peking Union Medical College Hospital, Chinese Academy of Medical Sciences and Peking Union Medical College, Beijing, China	Study concept or design
Zheng-Yu Jin, MD	Department of Radiology, State Key Laboratory of Complex Severe and Rare Diseases, Peking Union Medical College Hospital, Chinese Academy of Medical Sciences and Peking Union Medical College, Beijing, China	Study concept or design
Yi-Cheng Zhu, MD, PhD	Department of Neurology, State Key Laboratory of Complex Severe and Rare Diseases, Peking Union Medical College Hospital, Chinese Academy of Medical Sciences and Peking Union Medical College, Beijing, China	Drafting/revision of the manuscript for content, including medical writing for content; drafting/revision of the manuscript for content, including medical writing for content; major role in the acquisition of data; study concept or design; analysis or interpretation of data

References

1. Pantoni L. Cerebral small vessel disease: from pathogenesis and clinical characteristics to therapeutic challenges. *Lancet Neurol.* 2010;9(7):689-701. doi:10.1016/s1474-4422(10)70104-6
2. Rutten JW, Hack RJ, Duering M, et al. Broad phenotype of cysteine-altering NOTCH3 variants in UK Biobank: CADASIL to nonpenetrance. *Neurology*. 2020; 95(13):e1835–e1843. doi:10.1212/wnl.0000000000010525
3. Kang CH, Kim YM, Kim YJ, et al. Pathogenic NOTCH3 variants are frequent among the Korean general population. *Neurol Genet.* 2021;7(6):e639. doi:10.1212/nxg.0000000000000639
4. Rutten JW, Dauwerse HG, Gravesteijn G, et al. Archetypal NOTCH3 mutations frequent in public exome: implications for CADASIL. *Ann Clin Transl Neurol.* 2016; 3(11):844-853. doi:10.1002/acn3.344
5. Liu JY, Yao M, Dai Y, et al. Rare NOTCH3 variants in a Chinese population-based cohort and its relationship with cerebral small vessel disease. *Stroke*. 2021;52(12): 3918-3925. doi:10.1161/strokeaha.120.032265
6. Schmidt H, Zeginigg M, Wiltgen M, et al. Genetic variants of the NOTCH3 gene in the elderly and magnetic resonance imaging correlates of age-related cerebral small vessel disease. *Brain*. 2011;134(11):3384-3397. doi:10.1093/brain/awr252
7. Duering M, Zieren N, Herve D, et al. Strategic role of frontal white matter tracts in vascular cognitive impairment: a voxel-based lesion-symptom mapping study in CADASIL. *Brain*. 2011;134(8):2366-2375. doi:10.1093/brain/awr169
8. de Laat KF, Tuladhar AM, van Norden AG, Norris DG, Zwiers MP, de Leeuw FE. Loss of white matter integrity is associated with gait disorders in cerebral small vessel disease. *Brain*. 2011;134(1):73-83. doi:10.1093/brain/awq343
9. Phuah CL, Chen Y, Strain JF, et al. Association of data-driven white matter hyperintensity spatial signatures with distinct cerebral small vessel disease etiologies. *Neurology*. 2022;99(23):e2535-e2547. doi:10.1212/wnl.0000000000201186
10. Duchesnay E, Hadj Selem F, De Guio F, et al. Different types of white matter hyperintensities in CADASIL. *Front Neurol.* 2018;9:526. doi:10.3389/fneur.2018.00526
11. Ter Telgte A, van Leijsen EMC, Wiegertjes K, Klijn CJM, Tuladhar AM, de Leeuw FE. Cerebral small vessel disease: from a focal to a global perspective. *Nat Rev Neurol.* 2018;14(7):387-398. doi:10.1038/s41582-018-0014-y
12. Jouvent E, Mangin JF, Porcher R, et al. Cortical changes in cerebral small vessel diseases: a 3D MRI study of cortical morphology in CADASIL. *Brain*. 2008;131(8): 2201-2208. doi:10.1093/brain/awn129
13. van Leijsen EMC, van Uden IWM, Ghafoorian M, et al. Nonlinear temporal dynamics of cerebral small vessel disease: the RUN DMC study. *Neurology*. 2017;89(15): 1569-1577. doi:10.1212/wnl.0000000000004490
14. Lambert C, Benjamin P, Zeestraten E, Lawrence AJ, Barrick TR, Markus HS. Longitudinal patterns of leukoaraiosis and brain atrophy in symptomatic small vessel disease. *Brain*. 2016;139(4):1136-1151. doi:10.1093/brain/aww009
15. De Guio F, Duering M, Fazekas F, et al. Brain atrophy in cerebral small vessel diseases: extent, consequences, technical limitations and perspectives: the HARNESS initiative. *J Cereb Blood Flow Metab.* 2020;40(2):231-245. doi:10.1177/0271678x19888967
16. Han F, Zhou LX, Ni J, et al. Design of the Shunyi study on cardiovascular disease and age-related brain changes: a community-based, prospective, cohort study. *Ann Transl Med.* 2020;8(23):1579. doi:10.21037/atm-20-4195
17. Zhai FF, Yan S, Li ML, et al. Intracranial arterial dolichoectasia and stenosis: risk factors and relation to cerebral small vessel disease. *Stroke*. 2018;49(5):1135-1140. doi:10.1161/strokeaha.117.020130
18. Jenkinson M, Beckmann CF, Behrens TE, Woolrich MW, Smith SM. FSL. *Neuroimage*. 2012;62(2):782-790. doi:10.1016/j.neuroimage.2011.09.015
19. Winkler AM, Ridgway GR, Webster MA, Smith SM, Nichols TE. Permutation inference for the general linear model. *Neuroimage*. 2014;92:381-397. doi:10.1016/j.neuroimage.2014.01.060
20. Griffanti L, Zamboni G, Khan A, et al. BIANCA (Brain Intensity AbNormality Classification Algorithm): a new tool for automated segmentation of white matter hyperintensities. *Neuroimage.* 2016;141:191-205. doi:10.1016/j.neuroimage.2016.07.018
21. Greve DN, Fischl B. Accurate and robust brain image alignment using boundary-based registration. *Neuroimage*. 2009;48(1):63-72. doi:10.1016/j.neuroimage.2009.06.060
22. Andersson JLR, Jenkinson M, Smith S. *Non-linear Registration Aka Spatial Normalisation FMRIB Technical Report TR07JA2*. 2007. FMRIB Centre, Oxford.
23. Fischl B. FreeSurfer. *Neuroimage*. 2012;62(2):774-781. doi:10.1016/j.neuroimage.2012.01.021
24. Reuter M, Schmansky NJ, Rosas HD, Fischl B. Within-subject template estimation for unbiased longitudinal image analysis. *Neuroimage*. 2012;61(4):1402-1418. doi:10.1016/j.neuroimage.2012.02.084
25. Wardlaw JM, Smith EE, Biessels GJ, et al. Neuroimaging standards for research into small vessel disease and its contribution to ageing and neurodegeneration. *Lancet Neurol.* 2013;12(8):822-838. doi:10.1016/s1474-4422(13)70124-8
26. Vlachakis D, Tsaniras SC, Ioannidou K, Papageorgiou L, Baumann M, Kossida S. A series of NOTCH3 mutations in CADASIL; insights from 3D molecular modelling and evolutionary analyses. *J Mol Biochem.* 2014;3:134.
27. Smith SM, Nichols TE. Threshold-free cluster enhancement: addressing problems of smoothing, threshold dependence and localisation in cluster inference. *Neuroimage*. 2009;44(1):83-98. doi:10.1016/j.neuroimage.2008.03.061
28. Ramirez J, Dilliott AA, Binns MA, et al. Parkinson's disease, NOTCH3 genetic variants, and white matter hyperintensities. *Movement Disord.* 2020;35(11):2090-2095. doi:10.1002/mds.28171
29. Mishra A, Chauhan G, Violleau MH, et al. Association of variants in HTRA1 and NOTCH3 with MRI-defined extremes of cerebral small vessel disease in older subjects. *Brain*. 2019;142(4):1009-1023. doi:10.1093/brain/awz024
30. Santiveri CM, Santoro J, Rico M, Jimenez MA. Factors involved in the stability of isolated beta-sheets: turn sequence, beta-sheet twisting, and hydrophobic surface burial. *Protein Sci.* 2004;13(4):1134-1147. doi:10.1110/ps.03520704
31. Bolandzadeh N, Davis JC, Tam R, Handy TC, Liu-Ambrose T. The association between cognitive function and white matter lesion location in older adults: a systematic review. *BMC Neurol.* 2012;12(1):126. doi:10.1186/1471-2377-12-126
32. van den Heuvel DM, ten Dam VH, de Craen AJ, et al. Increase in periventricular white matter hyperintensities parallels decline in mental processing speed in a non-demented elderly population. *J Neurol Neurosurg Psychiatry*. 2006;77(2):149-153. doi:10.1136/jnnp.2005.070193